Exploring the effect of layer thickness on the elastoplastic properties of the constituent materials of CrN/CrAlN multilayer coatings: a nanoindentation and finite element-based investigation

Yamen Ben Ammar [a,*], Khalil Aouadi [b,c], Aurélien Besnard [d], Alex Montagne [e], Corinne Nouveau [d], Faker Bouchoucha [a]

[a] Laboratoire de recherche LR18ES45 sis à l'institut préparatoire aux études d'Ingénieur de Nabeul, Université de Carthage, Campus Universitaire, 8000, Mrezga, Tunisia
[b] Applied Mechanics and Systems Research Laboratory (LR03ES06), Tunisia Polytechnic School, University of Carthage, BP 743, Rue El Khawarizmi, La Marsa, 2078, Tunisia
[c] Morroccan Foundation for Advanced Science, Innovation and Research (MAScIR), Mohammed VI Polytechnic University (UM6P), Lot 660, Hay Moulay Rachid, 43150, Benguerrir, Morocco
[d] Arts et Metiers Institute of Technology, LABOMAP, HESAM Université, UBFC, F-71250, Cluny, France
[e] Université Polytechnique Hauts-de-France, LAMIH UMR 8201 CNRS, Mont Houy, 59313, Valenciennes, France

Keywords:
Instrumented-indentation testing
Multilayer coatings
Composite hardness modeling
Elasto-plastic properties
Inverse finite element material modelling

This paper aims to assess the effect of layer thickness on the elastoplastic properties of the constituent materials of multilayer coating systems, as well as on the stress and strain fields in the vicinity of the coating/substrate interface. A methodology based on a trust-region reflective optimization algorithm, integrated with finite element analysis of the nanoindentation process, is employed to extract the elastoplastic properties of the distinct layers, constituting multilayer coating. This approach is validated on a CrN/CrAlN multilayer coating systems with varying layer thicknesses from 1 to 0.35 μm, by which Young's modulus (E), yield stress (σ_y), and work hardening exponent (n) of each individual coating material layer were obtained. The results revealed a reduction in the hardness and Young's modulus of either CrN, or CrAlN coating layer as the layer thickness decreased. Finite element analysis of the nanoindentation process demonstrated that decreasing the coating layer thickness leads to an increase in the plastic deformation within the coatings, which reduces the stress concentration in this area. The simulation results suggest that an optimum thickness of 0.5 μm of CrAlN and CrN monolayer materials would improve the adhesion properties of CrN/CrAlN multilayer coatings.

1. Introduction

In recent years, the concept of multilayer nitride coatings has been proposed as a strategy to improve the performance of traditional monolayer nitride coatings [1–7]. Compared with monolayer nitride coatings, multilayer nitride coatings offer enhanced properties such as high hardness, high resistance to crack propagation resistance, and increased toughness. In general, the better performance of multilayer nitride coatings against wear damage, scratch and abrasion arises from the incorporation of alternating multilayer interface systems [1,2,5]. These can deflect cracks and impede their propagation, thus enhancing durability and protective capability of the coating.

Due to their remarkable capabilities, multilayer nitride coatings have become an important research topic in the last decade. Among these studies, a particular interest is given to optimizing the structure and type of multilayer nitride coatings to achieve coatings with the desired mechanical properties [2,4,7]. Based on the work of Kataria et al. [8], it's evident that the performance of multilayer nitride coatings is substantially dependent on the elastoplastic properties of the monolayers that constitute them. Furthermore, the distribution of residual stress and deformation at the coating/substrate interface, which control the tribological and adhesion properties of multilayer nitride coatings [1,9], is mainly related to the elastoplastic properties of monolayers of multilayer [10]. Therefore, determination of mechanical properties such as hardness, elastic modulus, yield stress, work hardening coefficient and fracture toughness of monolayers is necessary to achieve the design purposes [10,11]. Hence, it becomes essential to develop a methodology for extracting the elastoplastic properties of diverse layers within a

* Corresponding author.
E-mail address: yamen_benammar@yahoo.fr (Y.B. Ammar).

https://doi.org/10.1016/j.tsf.2024.140581

multilayer nitride coating. Furthermore, it is reported that the thickness and distribution of the metal layer play an important role in the mechanical and tribogical properties of the multilayer nitride coating [4,7,9,12,13]. However, there are insufficient investigations into the correlation between the layer thickness of multilayer nitride coatings and the elastoplastic properties of monolayers coatings, along with the mechanisms underlying this influence.

According to previous works [10,11,14], the assessment of the mechanical properties of multilayer coatings must be performed through nanoindentation under high indentation loads. This approach arises from the fact that the indenter must penetrate through the multiple layers of the coating to separate the contribution of each monolayer from the others and also from the substrate. In this context, numerous analytical models have been developed to predict the hardness and Young's modulus of monolayer coating systems from experimental load-penetration depth curves and composite hardness and composite modulus profiles [10,11,14–17]. However, in the context of multilayer coating, there has been limited development of comparable models that enable the simultaneous determination of intrinsic hardness of each individual layer, as well as the substrate. Among these models are the modified Jőnsson-Hogmark model [11], the modified Puchi Cabrera model [10] and the modified Korsunsky et al. model [10]. These models offer reasonably accurate predictions of the intrinsic hardness of individual layers and the substrate by taking into account the behavior of each layer (plastic deformation or fracture) and the substrate effect. Among these three models, special attention has been directed award the modified Jőnsson-Hogmark model. This model stands out for its minimal number of fitting parameters (just 2), and its high predictive performance compared to the other models [10].

Neverthless, these analytical models are unable to provide information about the elastoplastic properties of monolayers of the multilayer coating. In this instance, there are three kinds of approaches mainly used to characterize the elastoplastic properties of engineering materials and coating systems, dimensionless methods, machine learning methods, and finite element supported methods. The goal of the dimensionless analysis is to identify a constant or regular-change value among the attributes provided by nanoindentation [18]. DAO et al. [19] used a reverse analysis algorithm based on the dimensionless function, which can extract the elastoplastic properties of the pure and alloyed engineering metal from the indentation data. These dimensionless functions can help to establish the inverse method for the determination of elastic-plastic behavior from indentation curves. Xing et al. [20] performed a reverse analytical dimensionless algorithm to identify the elestoplastic properties of a ductile film on a hard substrate through nanoindentation for different ranges of penetration depth. Recently, Clayton et al. [21] established a dimensionnel analysis of instrumented dynamic spherical indentation combined with parametric finite element simulations to provide mechanical, thermal and rate-sensitivity properties of polycrystalline aluminum alloy Al 6061-T6.

FEM supported methods, especially when integrated with the experimental nanoindentation data, have been widely used to characterize the true elasticplastic properties of coatings on substrates. This approach has been employed to determine key parameters such as work hardening coefficient (n), Young's modulus (E) and yield stress (σ_Y) from the measured composite data [22–30]. Furthermore, the finite element method is considered an essential tool to investigate complex stress and strain fields within the coating and at the interface during nanoindentation in monolithic [25,31] and composite systems [3,32,33]. Understanding the stress and strain fields at the coating/substrate interface is primordially necessary to explain the crack formation and delamination phenomenon [3,32,33]. This understanding plays a critical role in deducing the elastoplastic properties of individual layers within multilayer coating.

The computation of the finite element analysis is designed to update the FE model of the indentation test iteratively by adjusting the FE model parameters until the best fit to the experimental nanoindentation P-h curve is found. In this context, Kang et al. [27] employed a non-linear least-squares optimization to extract a unique set of elastoplastic material properties, based on a single target load-displacement indentation curve. Nima and Iman [28] proposed a non-linear global optimization approach, fully integrated with FE analysis to characterize the elastoplastic properties of the HA film on Ti-6Al-4 V substrate. Furthermore, K. Bobzin et al. [29] obtained the plastic flow curves of CrN, AlN and CrN/AlN-multilayer coatings by combining nanoindentation and simulation. Recently, Wang et al. [30] developed a method to provide the anisotropic plastic properties of materials based on statistical Bayesian inference to address the inverse identification problem of material properties. Similary, Ammar et al. [23] proposed a method to address the uniqueness issue of the inverse analysis by estimating the initial guess parameters of the optimization procedure based on the Johnsson and Hogmark model. This method relies on finite element (FE) analysis and a trust-region reflective optimization algorithm to extract a unique set of elastoplastic properties of CrN monolayer coatings.

In recent years, with the advancement of computer technology and artificial intelligence, numerous research have combined machnine learning and nanoindentation to accurately assess the elastoplastic properties of engineering materials and coating systems. Wang et al. [34] used a hyperparametric tunable artificial neural network model to provide a relationship between the material elastoplastic properties and the indentation P-h curve of aluminium alloy Al 2024. For coating systems, Long et al. [35] established a long short-term memory neural network to deeply learn the time series of P-h curves to predict accurately the elastoplastic properties of metal-coated materials. Recently, Long et al. [36] proposed the convolutional neural network (CNN) to rapidly obtain the elastoplastic properties of coating systems with high prediction accuracy.

However, as mentioned above, research objects in these papers are common metal materials and monolayer coatings, and there is a lack of reported methods for identification of the elastoplastic properties of the constituent layers of multilayer coatings. Furthermore, most of these studies neglect the film thickness, the substrate effect, and the indentation size effect in their analysis, which can affect the reliability of the identified material properties.

The aim of the present work is to evaluate the effect of layer thickness on the elastoplastic properties of the constituant layer of multilayer thin films. To achieve this goal, a trust-region reflective optimization algorithm, based on the experimental nanoindentation data, has been devised for deducing a unique set of elastoplastic properties of each individual layer of the multilayer coating (Young's modulus, yield stress and work hardening coefficient). The uniqueness of this work lies in several aspects: the extraction of elastoplastic properties of the constituant layers of the multilayer coating, the evaluation of the effect of layer thickness on the elastoplastic properties of each monolayer and the knowledge of the stress and strain field at the coating/substrate interface, providing curtial information into the delamination properties of the multilayer coating system. The proposed methodology has been applied to a CrN/CrAlN multilayer coating system with various layer thicknesses. The results obtained from this work serve as a valuable reference for the structural optimization of multilayer coatings.

2. Experimental details

2.1. CrAlN/CrN multilayer coating deposition

The CrN/CrAlN multilayer coatings were deposited, with various layer thicknesses, on 90CrMoV8 steel samples ($20 \times 20 \times 5$ mm^3) using DC reactive magnetron sputtering. Before deposition, all substrates underwent ultrasonic cleaning in ethanol and after in acetone for 5 min in each, and then dried under compressed air. The chamber was heated at 300°C for 7 h, and the residual pressure was lower than 2×10^{-5} Pa. During deposition, the working pressure was set at 0.5 Pa, and the flow

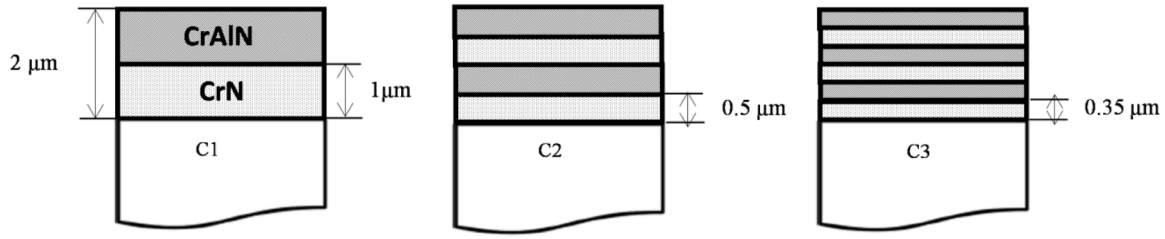

Fig. 1. Schematic illustration of CrN/CrAlN multilayer systems.

Table 1
Coating structures and thicknesses.

Conditions	Layers number		Layer thickness (µm)		Total thickness (µm)
	CrAlN	CrN	CrAlN	CrN	
C1	1	1	1	1	2 µm
C2	2	2	0.5	0.5	
C3	3	3	0.35	0.35	

rates of Ar and N_2 were 68.8 and 33.3 sccm, respectively. A chromium and aluminum target with a purity of 99.95 % and dimensions of (406.4 × 127 mm^2) was used for the deposition process. The chromium (Cr) and aluminum (Al) target power was set at 1500 W and 1000 W, respectively. The thickness of CrN and CrAlN underlayers was controlled by the deposition time. A substrate bias voltage of −500 V was applied, and the deposition time was fixed at 2 h. The substrate holder rotation was fixed at 1.5 rpm.

Fig. 1 shows the different multilayer coatings deposited in this study. Three multilayer coatings, denoted as C1, C2 and C3 were developed with a thickness gradient, choosing the same layer thicknesses used in the other coatings (1, 0.5, and 0.35 µm) and keeping the total thickness fixed around 2 µm. The thickness of each layer, the number of layers of each coating, and the total thickness of the coatings are presented in Table 1.

The microstructure of the CrN/CrAlN multilayer thin films featuring different layer thicknesses was observed by Scanning Electron Microscope (SEM) field emission (JEOL JSM7610F). The operational voltage was kept at 15 kV and its minimum spot size was approximately 1µm. Fig. 2 shows the microstructure of the multilayer coatings for C1, C2 and C3 conditions. All multilayer CrN/CrAlN coatings exhibit ovrall thickness around 2 µm and a columnar microstructure, which tends to decrease in size when the layer thickness decreases. A fine Cr underlayer of around 100 nm is deposited in the interface between the CrN/CrAlN thin films and the substrate in order to improve the adhesion strength of the structure by minimizing the internal stress.

2.2. Nanoindentation tests

The composite hardness (H) and the composite modulus (E) of CrN/CrAlN multilayer coatings were measured using nanoindentation tests with an XP instrument (MTS, USA) equipped with a Berkovich diamond tip. The tip radius of the indenter is about 200 nm, and its face angle is about 136°. For the continuous characterization of the composite hardness (H) and composite modulus (E) of the coating/substrate system, nanoindentation tests were performed using the CSM (Continuous Stiffness Measurement) mode. Each sample underwent nine indents with a maximum load of 750 mN. To investigate the impact of the substrate on the elastoplastic properties of the coating layers, large indentation depths surpassing the thickness of multilayer thin films (2 µm) were employed with a constant strain rate of 0.05 s^{-1}. The estimation of the hardness and Young's modulus of the constituant layers of multilayer thin films was performed through the modified (JH) model (Jőnsson-Hogmark model), which allows an evaluation of the monolayers and substrate hardness i.e. Young's modulus, separately from the measured composite hardness, i.e. composite modulus. The principle of the modified (JH) model will be detailed in the next section.

2.3. Estimation of the mechanical properties of multilayer coatings by the modified (JH) model

In this study, the modified (JH) model [10] was used to estimate the intrinsic hardness (H) and Young's modulus (E) of each monolayer composing the multilayer coating. In this model, the composite hardness (Hc) of a multilayer consisting of N layers is determined by a mixture law that relates the hardness of the i-layer ($H_f^{(i)}$) and the substrate (H_s):

$$H_c = \sum_{i=1}^{N} a_f{}^{(i)} H_f{}^{(i)} + a_f{}^{(s)} H_s \qquad ((1))$$

Where, $a_f{}^{(i)}$, represents the volume fraction of the i-layer of the multilayer coating, which contributes to the composite hardness (H_c). This volume fraction can be expressed for the first layer ($i = 1$) as a function of indentation depth, h, and the thickness of the first layer, $t_f^{(1)}$, by:

$$\begin{cases} a_f{}^{(1)} = 1 & \text{if } h < C^{(1)}\, t_f{}^{(1)} \\ a_f{}^{(1)} = 1 - \left(1 - \dfrac{C^{(1)}\, t_f{}^{(1)}}{h}\right)^2 & \text{Otherwise} \end{cases} \qquad ((2))$$

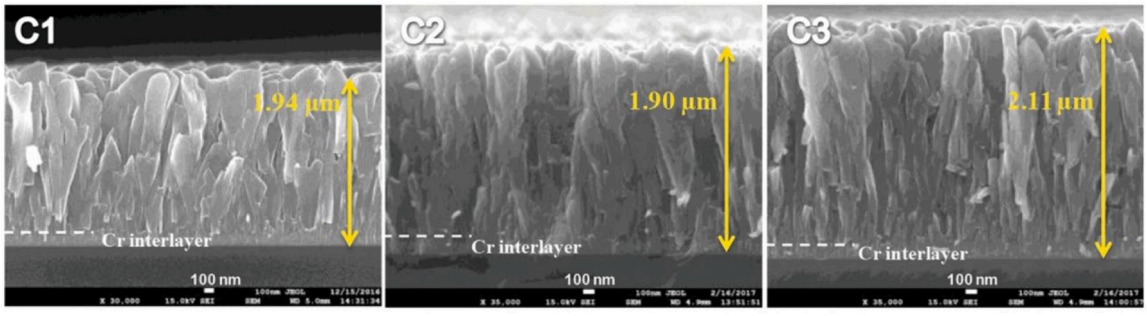

Fig. 2. Cross-sectional SEM images of the CrN/CrAlN multilayer coatings for C1, C2 and C3 conditions.

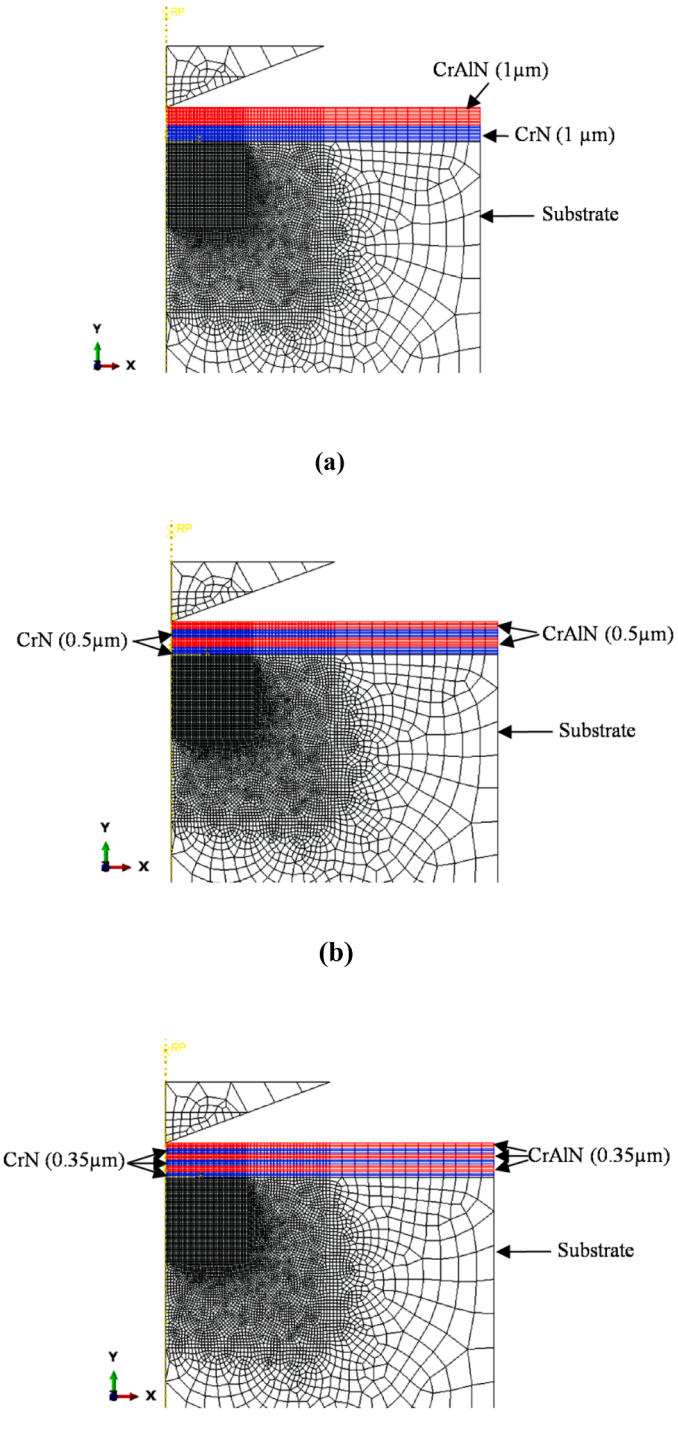

Fig. 3. FEM geometric model: magnified view of a dense mesh area close to the indenter contact: (a) 2 layers model (C1) (b) 4 layers model (C2) (c) 6 layers model (C3).

Where $C^{(1)}$, represents a constant depending on the indenter geometry and the indentation behavior of the layer under consideration [10]. In this model, the volume fraction of the coating material should be between 0 and 1. Consequently, if h is lower than $C^{(1)}\,t_f^{(1)}$, the substrate does not influence the composite hardness, and $a_f^{(1)}$ is equal to 1. Whereas, for the j^{th} layer of the coating, the volume fraction is expressed as follows:

$$\begin{cases} a_f{}^{(j)} = 1 - \sum_{i=1}^{j-1} a_f{}^{(i)} & if\, h < \sum_{i=1}^{j} C^{(i)}\, t_f{}^{(i)} \\ a_f{}^{(j)} = \left\{1 - \left\{1 - \dfrac{\sum_{i=1}^{j} C^{(i)}\, t_f{}^{(i)}}{h}\right\}^2\right\} - \left\{1 - \left\{1 - \dfrac{\sum_{i=1}^{j-1} C^{(i)}\, t_f{}^{(i)}}{h}\right\}^2\right\} & Otherwise \end{cases} \quad ((3))$$

Eq. (3) indicates that if $h > \sum_{i=1}^{j} C^{(i)} t_f{}^{(i)}$, the actual volume fraction of the j-layer contributing to the composite hardness can be calculated by subtracting the volume fraction of the preceding layer from that of the j-layer. Therefore, once the volume fraction of each layer has been determined, the volume fraction corresponding to the substrate material can be obtained:

$$a_f{}^{(s)} = 1 - \sum_{i=1}^{N} a_f{}^{(i)} \quad ((4))$$

Due to the indentation size effect (ISE), nanohardness is generally higher than the micro or macrohardnesses. To address this issue, the modified (JH) model was enhanced by incorporating the (ISE) effect. Using this model, the experimental composite hardness data can be described, and the macrohardness can be determined independently of the applied load for the i-layer ($H_{f0}^{(i)}$) and substrate (H_{S0}), assuming [10]:

$$H_f = H_{f0}{}^{(i)} + \frac{B_f{}^{(i)}}{h} \quad and \quad H_s = H_{s0} + \frac{B_s}{h} \quad ((5))$$

Where, B_f and B_s are the corresponding parameters for the (ISE).

Additionally, Young's modulus of the i-layer ($E_f^{(i)}$) and the substrate (E_s), are evaluated using the same model, considering C as a variable depending on the material [15,37]. Thus, for a multilayer coating, the composite modulus, E_c, would be given by Eq. (6):

$$E_c = \sum_{i=1}^{N} a_f{}^{(i)}\, E_f{}^{(i)} + a_f{}^{(s)} E_s \quad ((6))$$

where ($E_f^{(i)}$) represents Young's modulus of the i-layer, E_s represents Young's modulus of substrate and $a_f{}^{(i)}$ represents the volume fraction expressed by Eqs. (2) and (3).

Therefore, the modified (JH) model enables the description of the change in the composite hardness, i.e., composite modulus with penetration depth, for a multilayer system. Also, by means of non-linear least squares analysis, it allows the computation of the intrinsic hardness, i.e., Young's modulus of monolayers composing the multilayer, as well as that of the substrate.

2.4. Finite element modeling

In this study, the commercial finite element software Abaqus Standart 2017 was used to simulate the indentation process. The composite structure was modeled using over 8806 four-node axisymmetric elements with reduced integration (CAX4R).To simulate the semi-infinite substrate, the composite structure dimension was fixed to 25 × 70 µm^2. This model used X50CrMoV8–1 as substrate and featured CrN/CrAlN multilayer coatings with various layer number (2, 4 and 6 layers) and thicknesses (1, 0.5 and 0.35 µm), as illustrated in Fig. 3. The fine Cr underlayer is excluded from the model as its impact on the mechanical response of the composite structure is neglected. The total thickness of the multilayered structure remained unchanged at 2 µm. The mesh of the contact area was refined (0.1 µm x 0.1 µm) to improve the simulation accuracy. For the Berkovich indenter, an axisymmetric deformable conical indenter with a 70.3° face angle is used, giving the same projected area to depth-ratio as a Berkovich and Vickers indenters. The reduction of the 3D Berkovich model to axisymmetric one aims to simplify the numerical analysis and to accelerate the process of

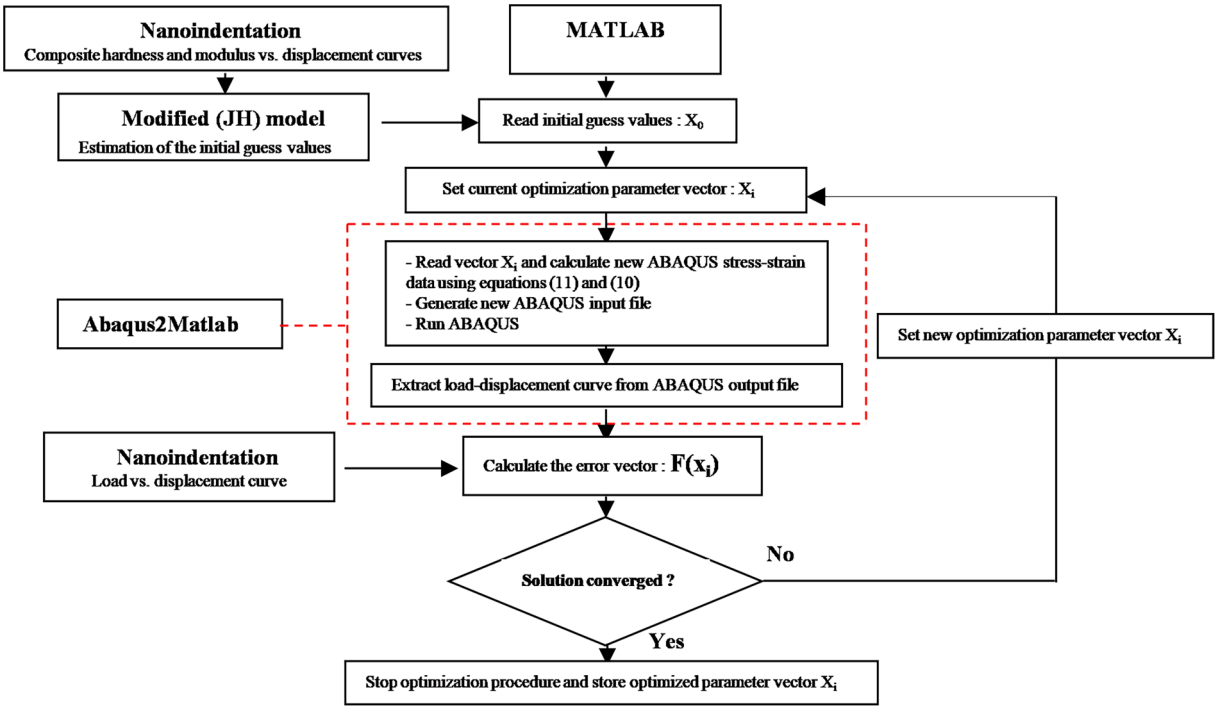

Fig. 4. Principle of the optimization procedure.

nanoindentation reverse analysis procedure. All the interfaces between materials in the composite structure were assumed to be perfectly bonded. The friction coefficients at the contact surfaces between the indenter and the top surface layer are assumed to be zero [23]. All nodes at the base of the specimen are constrained to prevent them from moving in the x and y directions. Indentation was applied in the finite element calculation by displacement control with a linear ramp in time and a final tip displacement equal to the experimental displacement measurement at maximum load.

The presented FE simulations are limited to modeling macro indentations and do not incorporate the indentation size effects.

2.5. Optimization analysis

2.5.1. Optimization algorithm

In this paper, a non-linear optimization algorithm is implemented using the MATLAB R-2019a optimization toolbox [38]. The connection between ABAQUS and MATLAB is provided through the software tool Abaqus2Matlab [39], enabling ABAQUS to be run directly from MATLAB and the simulated results to be post-processed. The proposed optimization algorithm seeks to identify the optimal elastoplastic properties of the monolayers in a multilayer coating by reducing the error between the experimental indentation load-displacement data and the FE simulated data using an iterative procedure based on a MATLAB nonlinear least-squares routine (called LSQNONLIN). This routine, based on the trust-region reflective algorithm [38], proves efficient in solving bound-constrained nonlinear minimization problems and enables to avoid the impractical values and to ensure the accuracy of results by setting the upper and lower bound constraints for the material variables. Thus, the prediction error in indentation depth is evaluated iteratively at each load increment point (i), summed, and minimized to produce the best fit between the experimental and the simulated indentation data. To achieve this goal, a cost function F(X), which describes the error criteria, is minimized until a minimum convergence value within the range of 10^{-2} is reached. The cost function is expressed by Eq. (7):

$$F(X) = \frac{1}{2}\sum_{i=1}^{N}\left[P(X)_i^{pre} - P_i^{\exp}\right]^2 \rightarrow \min \qquad ((7))$$

$$X \in R^n$$

$$LB \leq X \leq UB$$

Where X are the elastoplastic properties:$X = \left[elastoplastic\ properties\ (E,\sigma_y,n)\right]$, which are starting from an initial guess parameter$X_0 = [elastoplastic\ properties\ (E_0,\sigma_0,n_0)]$. N is the total number of points used in the measured load-displacement loop. LB and UB represent the lower and upper boundaries constraints of elastoplastic properties X, and $P(x)_i^{pre}$ and$P_i^{\exp}$ represent the simulated and the experimental total force, respectively, at specific position i, within the loops.

2.5.2. Optimization procedure

In this study, the elastoplastic properties (Young's modulus, yield stress and work hardening exponent) of monolayers, forming the multilayer coating, were parameterized in the ABAQUS input files and adjusted at each iteration of the optimization to generate new input files. By using the software tool Abaqus2Matlab for interfacing, ABAQUS will be executed for calculation from Matlab, and the simulated load-displacement curves will be extracted from the resulting ABAQUS output files.

In the simulation, the diamond Berkovich indenter was modeled as an elastic, perfectly plastic material with a Young's modulus, $E = 1024$ GPa, a Poisson ratio, υ=0.07, and a yield stress, $\sigma_y = 35.7$ GPa [40]. For the monolayer materials and the substrate, a power law work hardening curve was used to simulate the indentation experiments. The stress-strain (σ-ε) relationship can be described as:

$$\sigma = \begin{cases} E\varepsilon \quad for \quad \varepsilon \leq \dfrac{\sigma_y}{E} \\ K\varepsilon^n \ for \quad \varepsilon > \dfrac{\sigma_y}{E} \end{cases} \qquad ((8))$$

where E is Young's modulus, σ_y represents the yield stress, n is the work hardening coefficient and K represents the strength coefficient.

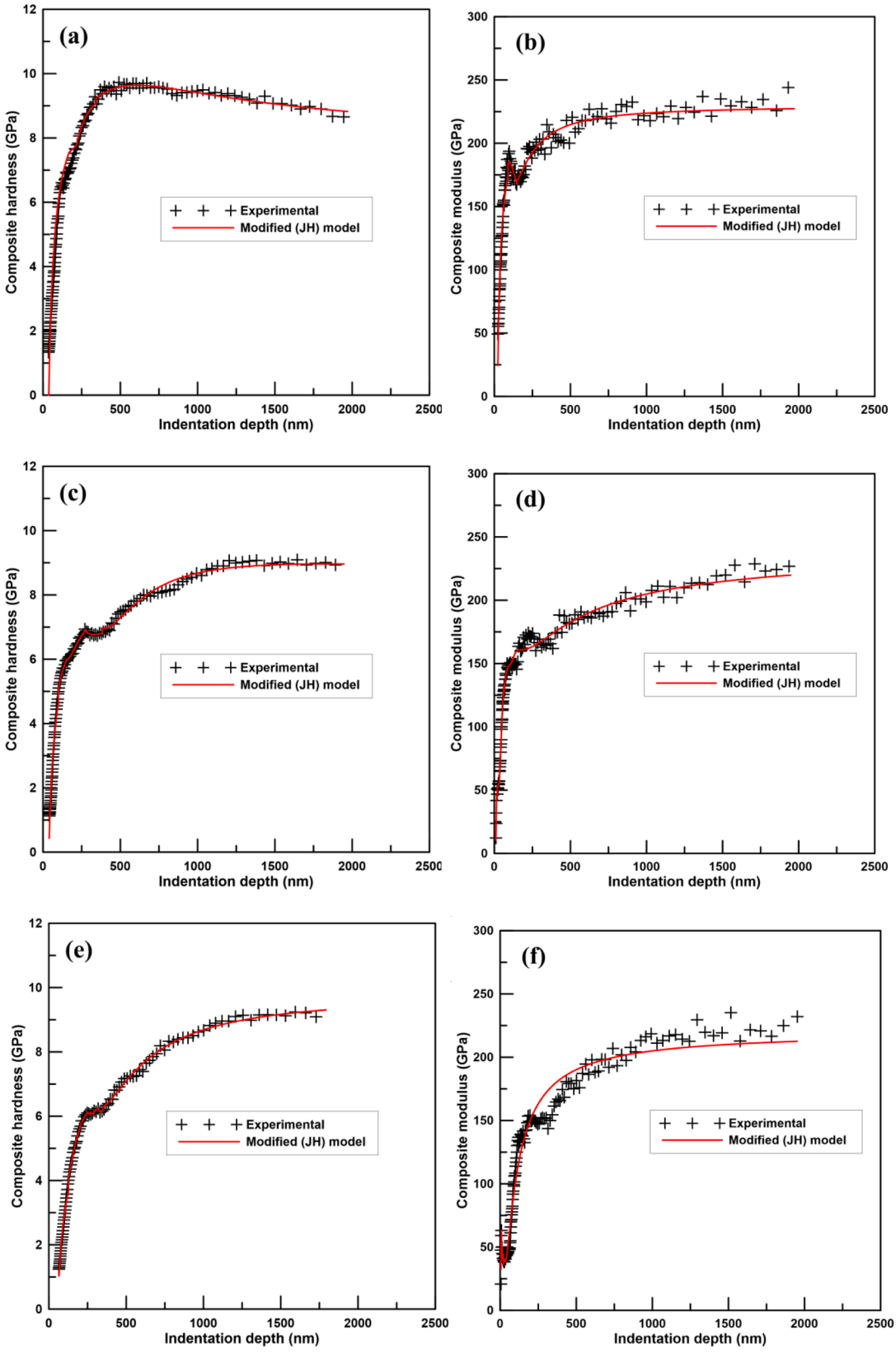

Fig. 5. Profile of the composite hardness and composite modulus as a function of the penetration depth for the CrN/CrAlN multilayer coating systems: (a, b) C1; (c, d) C2 and (e, f) C3.

Table 2
Materials properties obtained by the modified (JH) model.

Conditions	Materials	H (GPa)	σ_y (GPa)	E (GPa)
C1	CrAlN	9.68	3.22	221.41
	CrN	5.92	1.98	121.12
	Substrate	7.72	2.57	218.51
C2	CrAlN	7.63	2.54	127.2
	CrN	4.86	1.65	92.2
	Substrate	8.32	2.77	233.23
C3	CrAlN	6.45	2.15	118.82
	CrN	4.05	1350	66.34
	Substrate	8.78	2.92	220.26

The decomposition of the strain into elastic and plastic parts is given by:

$$\varepsilon_{total} = \varepsilon_{el} + \varepsilon_{pl} \quad ((9))$$

Then, the stress equation can be written as:

$$\sigma = K\left(\frac{\sigma_y}{E} + \varepsilon_{pl}\right)^n \quad ((10))$$

where K can be expressed by:

$$K = E^n \sigma_y^{1-n} \quad ((11))$$

Thus, to define the plastic stress-strain data in the ABAQUS input file, the optimization algorithm calculates firstly the coefficient K through Eq. (11) and updates the stress data related to each plastic strain value through Eq. (10).

The principle of the optimization procedure used in this work is shown in Fig. 4. The proposed optimization approach can be described in the following steps:

- Firstly, the modified (JH) model is used to estimate the hardness and Young's modulus of monolayers of the multilayer coating and the substrate from the composite hardness and the composite modulus profiles obtained by nanoindentation experiment.
- Secondly, the estimated values of hardness were used to estimate the yield stress of monolayers and substrate using the Tabor assumption derived for metals [41], H/c, where c is a constant which is normally taken as 3 for ideal plastic materials undergoing sharp indentation.

Table 3
Optimization results.

Systems	Materials	Optimization parameter	Initial guess parameter	Bound constraints	Optimized parameters	Iterations
C1	CrAlN	(E)	221.41 [GPa]	50<E[GPa]<240	192.17 [GPa]	13
		(σ_y)	3.22 [GPa]	1<σ_y[GPa]<14	3.15 [GPa]	
		(n)	0.2	$0 < n < 0.5$	0.33	
	CrN	(E)	121.12 [GPa]	50<E[GPa]<240	128.32 [GPa]	
		(σ_y)	2 [GPa]	1<σ_y[GPa]<14	2.42 [GPa]	
		(n)	0.2	$0 < n < 0.5$	0.29	
C2	CrAlN	(E)	127.2 [GPa]	50<E[GPa]<240	131.1 [GPa]	19
		(σ_y)	2.54 [GPa]	1<σ_y[GPa]<14	2.97 [GPa]	
		(n)	0.2	$0 < n < 0.5$	0.23	
	CrN	(E)	92.2 [GPa]	$50 < E$[GPa] < 240	98.4 [GPa]	
		(σ_y)	1.65 [GPa]	$1 < \sigma_y$[GPa] < 14	2.21 [GPa]	
		(n)	0.2	$0 < n < 0.5$	0.21	
C3	CrAlN	(E)	118.82 [GPa]	$50 < E$[GPa] < 240	127.29 [GPa]	22
		(σ_y)	2.15 [GPa]	$1 < \sigma_y$[GPa] < 14	2.63 [GPa]	
		(n)	0.2	$0 < n < 0.5$	0.37	
	CrN	(E)	66.34 [GPa]	$50 < E$[GPa] < 240	75.23 [GPa]	
		(σ_y)	1.4 [GPa]	$1 < \sigma_y$[GPa] < 14	2.04 [GPa]	
		(n)	0.2	$0 < n < 0.5$	0.38	

Table 4
Literature data on the mechanical properties of CrN coatings.

	Values	thickness (μm)	Deposition technique	Substrate	Model
H (GPa)	26 [47]	0.8	DC–PVD*	stainless steel	Olivar and Phar (nanoindentation tests)
	24 [29]	2	DC–PVD	cemented carbide	
	19 [48]	1.3	RF–PVD**	silicon	
	16 [49]	1	DC–PVD	silicon	
	13 [50]	0.3	RF–PVD	metallic glass	
	12 [51]	0.6	DC–PVD	silicon	
	10 [52]	0.3	RF–PVD	metallic glass	
	8.5 [42]	2	DC–PVD	stainless steel	Microhardness test
	5 [42]	2	DC–PVD	stainless steel	
	3–22 [53]	4–5	DC-PVD	stainless steel	
E (GPa)	437 [29]	2	DC-PVD	cemented carbide	Olivar and Phar (nanoindentation tests)
	360 [47]	0.8	DC-PVD	stainless steel	
	235 [51]	0.6	DC-PVD	silicon	
	170 [49]	1	DC-PVD	silicon	
	160 [50]	0.3	RF-PVD	metallic glass	
	100 [52]	0.3	RF-PVD	metallic glass	
	102 [23]	1	DC-PVD	stainless steel	Finite element inverse analysis
	185 [26]	1	DC-PVD	silicon	
σ_y (GPa)	12 [26]	1	DC-PVD	silicon	Finite element inverse analysis
	4 [50]	0.3	RF-PVD	metallic glass	
	2 [29]	2	DC-PVD	cemented carbide	
	1.7 [23]	1	DC-PVD	stainless steel	

* DC-PVD: direct current (DC) plasma assisted PVD.
** RF-PVD: radio-frequency (RF) plasma assisted PVD.

Table 5
Literature data on the mechanical properties of CrAlN coatings.

	Values	Thickness (μm)	Deposition technique	Substrate	Model
H (GPa)	18–24 [54]	0.6	DC–PVD	silicon	Olivar and Phar (nanoindentation tests)
	17 [55]	3.45	RF–PVD	silicon	
	28 [56]	3.3	DC–PVD	M2 steel	
	14 [57]	0.2	MF–PVD*	silicon	
	22 [58]	2.8	DC–PVD	stainless steel	
	6.5 [59]	1.1	DC–PVD	silicon	
	12–20 [60]	1.5	(DC+HPP)–PVD**	High speed steel	
	18–30 [61]	1.9–3.8	DC-PVD	cemented carbide	
E (GPa)	225–255 [54]	0.6	DC–PVD	silicon	Olivar and Phar (nanoindentation tests)
	315 [55]	3.45	RF–PVD	silicon	
	235 [56]	3.3	DC–PVD	M2 steel	
	377 [58]	2.8	DC–PVD	stainless steel	
	180 [59]	1.1	DC–PVD	silicon	
	254–317 [60]	1.5	(DC+HPP)–PVD	High speed steel	
	380–530 [61]	1.9–3.8	DC-PVD	cemented carbide	
σ_y (Gpa)	5.7 [59]	1.1	DC–PVD	silicon	Finite element inverse analysis
	13 [60]	1.5	(DC+HPP)–PVD	High speed steel	
	1–5 [61]	1.9–3.8	DC-PVD	cemented carbide	Juliano method [62]

* MF-PVD: mid-frequency (MF) plasma assisted PVD.
** (DC+HPP)-PVD: a hybrid direct current (DC) and high power pulse (HPP) plasma assisted PVD.

Thus, the estimated values of Young's modulus and yield stress of monolayers are used to define the intial guess parameter vector $X_0 = [elastoplastic\ properties\ (E_0, \sigma_0, n_0)]$ in the optimization procedure. Neverless, the initial value of the work hardening coefficient n_0 of monolayers will be set arbitrary.

- Thirdly, the intial guess parameters X_0 of each monolayer were substituted into the finite element model calculation, and the error between the simulated and the experimental load-displacemet curves was calculated through the cost function F(X) (Eq. (7)), and minimized iteratively by modifying the elastoplastic properties $X = [elastoplastic\ properties\ (E, \sigma, n)]$ of monolayers. Hence, when the convergence condition reached the specified tolerance (10^{-2}), the optimization process would be completed, and the optimal elastoplastic properties of each monolayer would be determined from which the best fit between the experimental and simulated load-displacement curves can be achieved.

In this study, there are six unknown elastoplastic properties to optimize for each multilayer coating system (C1, C2 and C3): E^{CrAlN}, σ^{CrAlN}, n^{CrAlN}, E^{CrN}, σ^{CrN}, n^{CrN}. The poisson ratio υ of CrAlN and CrN is assumed to be equal and constant of magnitude of 0. 22 [42]. To reduce the number of unknown parameters in the the model, the elastoplastic properties of the substrate are fixed in the simulation model, assuming that Young's modulus and the yield stress are equal to the estimated values measured by the modified (JH) model and the Tabor assumption, respectively. For the substrate, the work hardening coefficient (n) and the poisson ratio (υ) are assumed to be equal to 0.1 and 0.3 [43], respectively.

Thus, three optimization processes will be performed to determine the optimal elastoplastic properties (E, σ_y and n) of CrAlN and CrN monolayers, constituting the multilayer coating systems: C1, C2 and C3.

2.5.3. The uniqueness of the solution

In this work, the trust region algorithm, in cooperation with the modified (JH) model, is used to determine a unique set of six elastic-plastic parameters (E^{CrAlN}, σ^{CrAlN}, n^{CrAlN}, E^{CrN}, σ^{CrN}, n^{CrN}), using results from a single indentation curve. Neverless, extracting a unique set of more than two unknown elastoplastic properties from a single indentation test has proven to be difficult [22,26,27].

To circumvent the challenges mentioned earlier, some researchers [26,27] propose to use multiple (P-h) curves obtained from independent indenter shapes. Other authors [20,22] suggest utilizing (P-h) curves obtained by different maximum indentation depths. An alternative approach as proposed by other researchers [23,27,43] involves selecting initial guess properties that are closer to the target values and narrowing the range of the initial guess properties using a set of bound constraints (lower and upper bound) for each variable. This approach aims to limit the space of possible solutions during the optimization. Furthermore, it is reported that convergence is faster, and with improved accuracy, when the initial guess values are chosen closer to the target values [27, 44,45].

In this study, the non-uniqueness issue is addressed through two strategies; firstly, the initial elastoplastic properties are chosen nearly to the target values using the estimated elastoplastic properties provided by the modified (JH) model; Secondly, the space of possible solutions is limited by using lower and upper boundaries for each variable. The bound constraints are adjusted based on the literature data. Hence, only two elastoplastic properties will be set arbitrary: the strain hardening coefficient of CrAlN and CrN (n^{CrAlN} and n^{CrN}).

3. Results and discussion

3.1. Estimation of the initial guess properties by the modified (JH) model

Fig. 5 shows the variation of the experimental composite hardness and composite modulus of the three CrN/CrAlN multilayer coating systems: C1, C2 and C3, as a function of the penetration depth. The modified (JH) model is used to describe these experimental curves, assuming for the determination of hardness (H) that the monolayers CrAlN and CrN tend to deform plastically by setting C to 0.1746 [11]. Hence, the hardness of the monolayers and the substrate is evaluated by fitting the experimental data through a non-linear least-squares optimization MATLAB function fminsearch (see Fig. 5). The identical procedure is employed to determine their Young's modulus in which the constant C is also optimized. Furthermore, the yield stress (σ_y) of the monolayer materials and the substrate is estimated using the estimated value of hardness through the Tabor assumption (see Section 2.5.2). Table 2 summarizes the estimation results of materials properties obtained by the modified (JH) model for the three multilayer coating systems: C1, C2 and C3. As can be observed in Fig. 5, the modified (JH) model provides a reaisonable description of the variation in the composite hardness and composite modulus of the multilayer coating systems as a function of the penetration depth. The model results show a decrease in the mechanical properties of the CrAlN and CrN monolayer coatings when their thickness decreases.

For the steel substrate, the mean value of Young's modulus calculated from the three estimated values in Table 3 is equal to 225 GPa which is coherent with the literature data (E between 190 GPa and 215

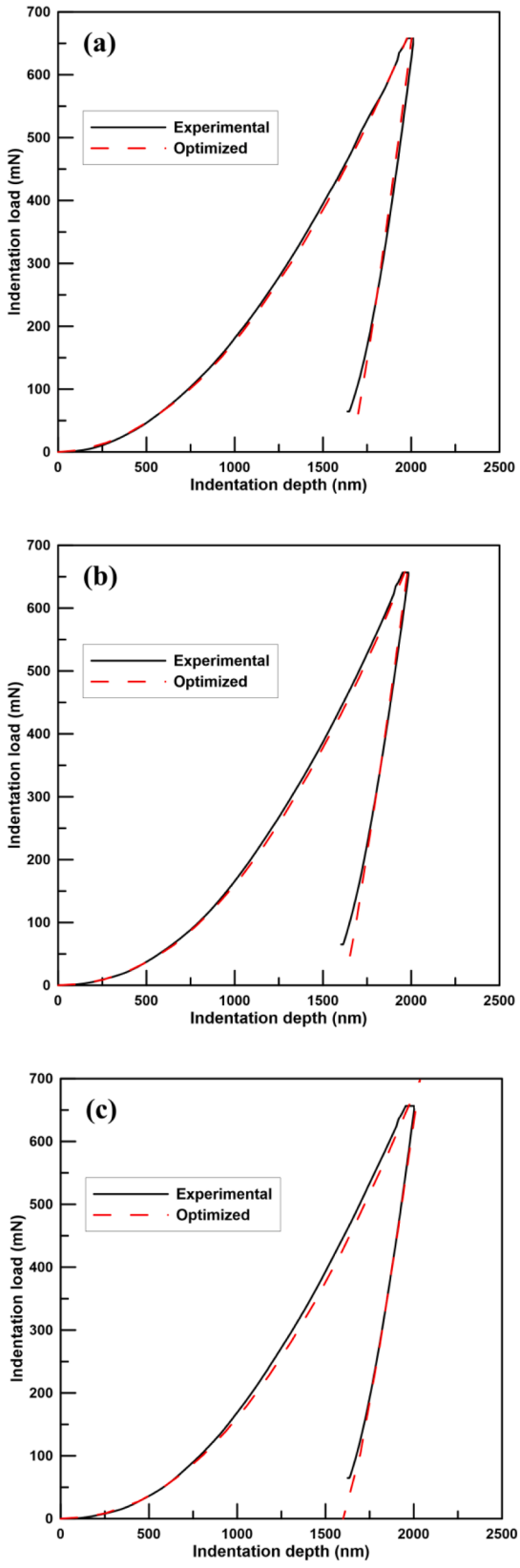

Fig. 6. Comparison of experimental (P-h) curves and the simulated ones using the optimal elastoplastic properties of CrAlN and CrN monolayers of the multilayer coating systems: (a) C1; (b) C2; (b) C3.

GPa). Moreover, the mean value of hardness of the steel substrate calculated from the values predicted by the modified (JH) model (see Table 3 in the paper) is equal to 8 GPa, which is coherent with the value reported in literature data $H = 7$ GPa [46] (measured by the mico-rhardness test).

3.2. *Optimization results*

In this study, the proposed optimization procedure is validated on a CrN/CrAlN multilayer coating system with various layer thicknesses. Through this process, the optimal elastoplastic properties (E, σ_y and n) of CrAlN and CrN monolayers are extracted. The optimization results are shown in Table 3. The initial guess parameters of the optimization procedure are determined using the outcomes from the modified (JH) model results (see Table 2). The initial value of the work hardening coefficient (n) of monolayers was arbitrary chosen, between 0.0 and 0.5. Additionally, the material parameters of the substrate remain fixed in the simulation. The yield stress (σ_y) and Young's modulus (E) are assumed to be equal to the values estimated by the modified (JH) model (as shown in Table 2). Moreover, to ensure the accuracy of the results, the lower and upper boundaries of each variable are adjusted based on the literature data (Tables 4 and 5). Assuming that the mechanical properties of CrAlN and CrN monolayers are close, the same lower and upper boundaries of their properties are used.

Fig. 6 illustrates the comparison between the experimental (P-h) curves and the simulation (P-h) curves using the optimal solution of elastoplastic properties of each monolayer of the multilayer coating systems C1, C2 and C3. The simulation curves correspond closely to the experimental ones, proving the high reliability of the proposed optimization procedure. Furthermore, upon comparing the optimal solution of (E) and (σ_y) for the CrAlN and CrN monolayers with their initial values (Table 3), we can conclude that the variation was generally less than 20 % with a high convergence rate of approximately less than 20 iterations, indicating the accuracy of the proposed methodology.

3.3. *Effect of layer thickness on the elastoplastic properties of CrAlN and CrN monolayer materials*

The optimization process determined the elastoplastic properties of CrAlN and CrN monolayers for various layer thicknesses (1, 0.5 and 0.35 μm). Fig. 7 shows the variation of (E) and (σ_y) of CrAlN and CrN monolayers as a function of layer thickness. As can be seen in Fig. 7, regardless of the layer thickness, the mechanical properties of the CrAlN monolayer are higher than those of the CrN monolayer. This is due to the incorporation of Al in the cubic lattice of CrN system, which improves mechanical properties [4]. The mechanical properties of CrN monolayers that have been found in this work are in good agreement with those found in the last work [23]. The uniqueness of this identification procedure is to consider the substrate effect in the calculation of mechanical properties of films. Indeed, previous studies overlook this factor and use the Oliver-Pharr method [63] in the evaluation of the mechanical properties of CrAlN and CrN monolayers (Tables 4 and 5).This method measures the mechanical properties of the coating using nano-indentation (P-h) curves, assuming that the proper value corresponds to penetration depth less than 10 % of the coating thickness. However, this measurement is strongly affected by many factors, such as the coating surface roughness and the phenomena called skin-in and pile-up, which can result in an underestimation of the contact area and consequently an overestimation of the hardness and Young's modulus of the coatings (Tables 4 and 5) [55,64,65]. Thus, it's necessary for the determination of the true mechanical properties of a given coating to separate the contribution of the coatings from the substrate [10]. Furthermore, another factor can affect the evaluation of the mechanical properties of the coatings, which is the indentation size effect (ISE). Indeed, this phenomenon involves an increase in hardness and Young's modulus when the indentation size (layer thickness) decreases [65]. For the

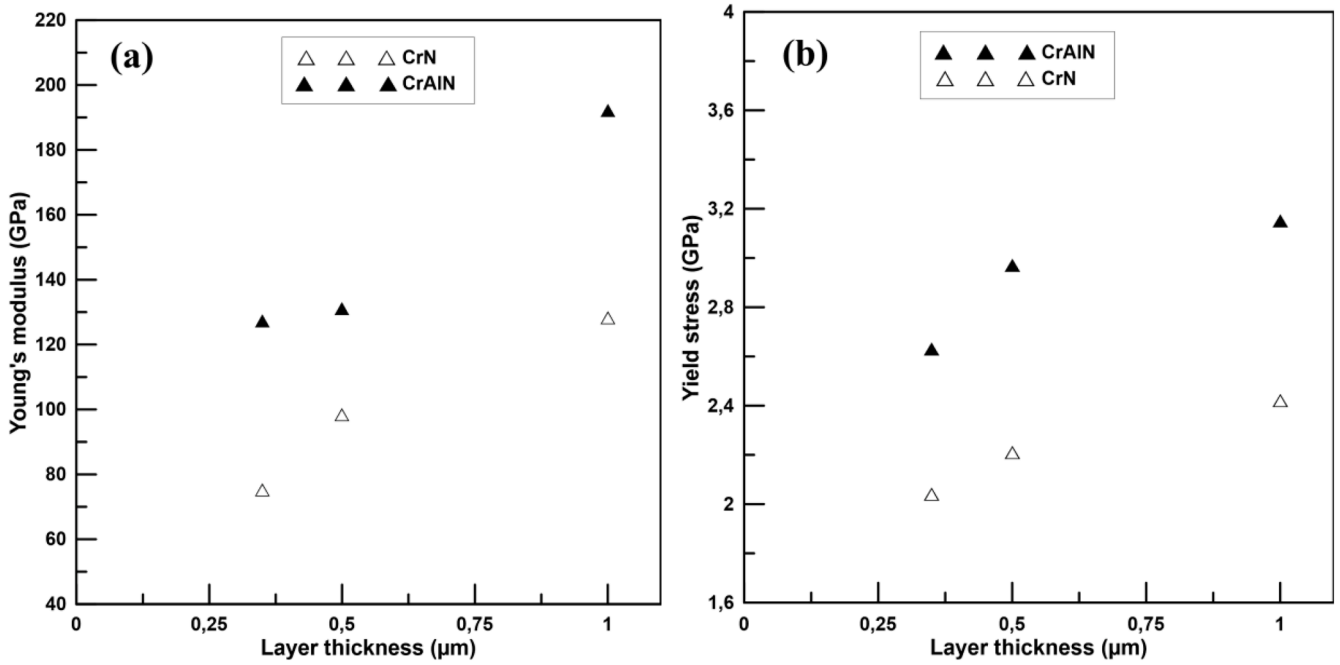

Fig. 7. Variation of: (a) Young's modulus, and (b) yield stress of CrAlN and CrN monolayer materials as a function of the layer thickness.

Table 6
(H/E) and (H^3/E^2) ratio results as a function of CrAlN and CrN layer thickness.

Monolayers	Thickness layer (μm)	H/E	H^3/E^2
CrAlN	1	0.050	0.024
	0.5	0.058	0.025
	0.35	0.050	0.016
CrN	1	0.046	0.012
	0.5	0.049	0.012
	0.35	0.053	0.011

multilayered systems, the evaluation of the mechanical properties is usually conducted through the Oliver-Pharr method. Neverless, the measurement results will be dominated by the mechanical properties of the top layer coating and by its thickness. Under these conditions, this method is not capable of providing a reasonable evaluation of the mechanical properties of the entire multilayer coatings [66]. Hence, it's recommended to evaluate the mechanical properties of monolayers rather than the whole multilayer coating.

In this study, results show a decrease in Young's modulus (E) and yield stress (σ_y) of CrAlN and CrN monolayer materials when their layer thickness decreases. Indeed, Young's modulus of CrAlN and CrN monolayers drops from 192.17 GPa and 128.32 GPa for a layer thickness of 1 μm to 127. 29 GPa and 75.23 GPa for a layer thickness of 0.35 μm, respectively.The same trends are observed for their yield stress which decreases from 3.15 GPa to 2.63 GPa for the CrAlN monolayer and from 2.42 GPa to 2.04 GPa for the CrN monolayer. Comparable results for the multilayered system CrN/CrAlN are reported in [67], which indicate a decrease in the hardness and Young's modulus of the CrN/CrAlN composite systems when decreasing the layer thickness and the number of monolayer materials.

3.4. Effect of layer thickness on the adhesion properties of CrAlN and CrN monolayer coatings

Many factors impact the adhesion properties of the coating, including substrate surface roughness, deposition conditions, and coating thickness [68–70]. The evaluation of the adhesion properties of the coating is usually performed using the ratio of hardness and Young's modulus (H/E), which represents the resistance to elastic deformation, and also the ratio (H^3/E^2) which represents the resistance to plastic deformation. The last one is reported as the suitable criteria to evaluate the adhesion properties and the wear resistance of the coating [69]. To assess the effect of layer thickness on the adhesion properties of CrAlN and CrN monolayers, the ratios (H/E) and (H^3/E^2) are computed for each monolayer using the data from Tables 2 and 3. The corresponding results are reported in Table 6. It's clear that the ratio results (H/E) and (H^3/E^2) calculated for the CrAlN monolayer are higher than those of CrN monolayer, independently from the layer thickness. These results revealed the higher adhesion properties of CrAlN monolayer compared with the CrN monolayer. Furthermore, the results indicate that the (H^3/E^2) ratio increases as the coating thickness decreases from 1 μm to 0.5 μm and then begins to decline up to 0.35 μm for both CrAlN and CrN monolayer films. These results suggest that there is a critical layer thickness of 0.5 μm at which the adhesion properties of the CrAlN and CrN monolayer coatings are improved. Hence, the multilayer coating system C2 with a monolayers thickness of 0.5 μm exhibits the best adhesion properties. Comparable results are found in the last work [4], which indicates an increase in the adhesion properties of the CrN/CrAlN multilayer coating when decreasing the layer thickness and the layer number.

3.5. Analysis of the stress and strain distribution at the coating/substrate interface

In this study, FEM combined with the experimental nanoindentation data was employed to analyze the stress and deformation distribution within the coating/substrate system. These methods have been used successfully in the past to investigate the local stress and the deformation process during nanoindentation in monolayer and multilayer coatings [71–72]. Also, it's used to evaluate the failure in the coated system by characterizing the crack initiation and propagation, using as a criteria either critical stress or energy [70–71]. According to Bahri et al. [72], the crack initiation and propagation within the coating can be correlated to the stress distribution under the loading phase of nanoindentation process.

In this work, the effect of CrAlN and CrN layer thickness on the stress and strain distribution within the multilayer coating systems C1, C2 and

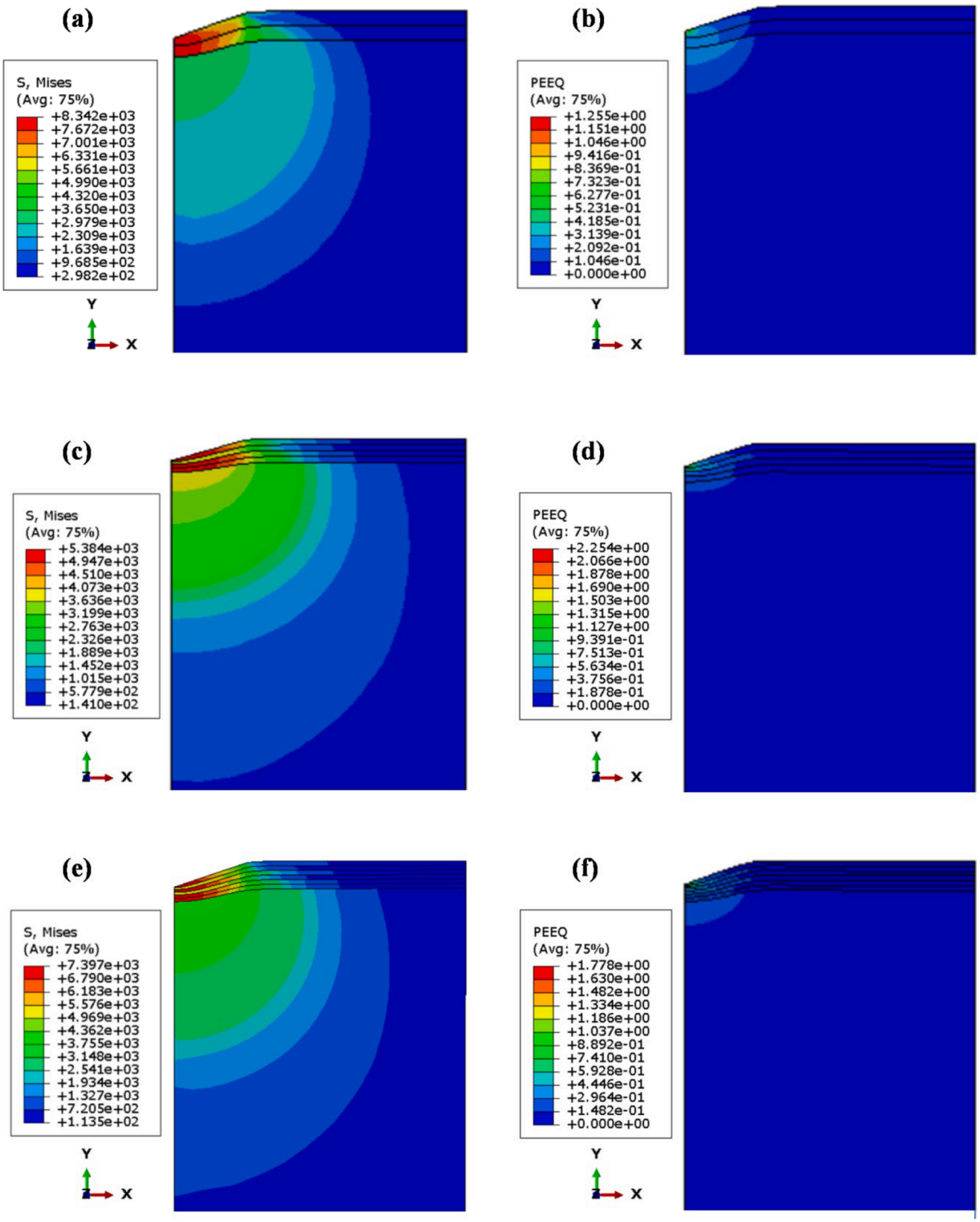

Fig. 8. Distribution of von Mises stress after loading and equivalent plastic strain after unloading within the CrN/CrAlN multilayer coating systems: (a) and (b) C1, (c) and (d) C2, (e) and (f) C3.

C3 was investigated by visualizing the distributions of von Mises stresses after the loading stage and equivalent plastic strains after the unloading stage.

Fig. 8 depicts the distribution of von Mises stress at a maximum indentation depth of 2 μm and equivalent plastic strain after unloading within the CrN/CrAlN multilayer coating systems: C1, C2 and C3.

As illustrated in Fig. 8(a), (c) and (e), the stress field was located inside the monolayer coatings. The highest value of stress is observed in the multilayer coating system C1 while the multilayer coating system C2 presents the lowest one. These results indicate that decreasing monolayer layer thickness reduces the stress concentration within the multilayer coating. Furthermore, as shown in Fig. 8(b), (d) and (f), the maximum equivalent plastic strain within the multilayer coating increases when the layer thickness of monolayers decreases. This indicates that the plastic deformation reduces the stress level within the multilayer coatings. Moreover, the results confirm that the multilayer coating system C2 with a monolayer thickness of 0.5 μm exhibits the lowest stress concentration and the highest plastic deformation value, which reveals the best adhesion properties of this system. This finding aligns with the results found in the previous section, suggesting that the performance of multilayer coatings is mainly dependent on the elastoplastic properties of the monolayers that constitute them.

In this work, the elastoplastic properties of CrAlN and CrN monolayers were evaluated for different layer thicknesses. In the further study, the focus will be to characterize the damage behavior of these monolayers using scratch test results. The correlation between finite element modeling results and the experimental results of the scratch test would be used to analyze the effect of layer thickness and the number of inerface layers on the damage behavior of the multilayer coatings.

4. Conclusions

In this study, CrN/CrAlN multilayer coatings with various layer thicknesses were prepared using PVD technology. The influence of layer thickness on the elastoplastic properties of the constituent materials of the multilayer coating was investigated through nanoindentation using a trust-region optimization algorithm integrated with numerical indentation models. The efficiency of the proposed optimization procedure to determine a unique set of elastoplastique properties of the constituent materials of multilayer coating is supported and validated by its efficiency to fitting the experimental nanoindentation (P-h) curves. The optimization results show that the hardness and Young's modulus of CrAlN and CrN monolayers decrease when decreasing the layer thickness. By using the relation (H^3/E^2) as criteria, the best adhesion properties for CrAlN and CrN monolayers were found for a layer thickness of 0.5 μm. The simulation results of CrN/CrAlN multilayer coating nanoindentation model show an increase in the plastic deformation within the coating when the layer thickness decreases, which reduces the stress concentration in this area and improves the adhesion properties of CrN/CrAlN multilayer.

CRediT authorship contribution statement

Yamen Ben Ammar: Writing – review & editing, Writing – original draft, Visualization, Validation, Software, Investigation, Formal analysis, Data curation, Conceptualization. **Khalil Aouadi:** Writing – original draft, Validation, Methodology, Investigation, Data curation. **Aurélien Besnard:** Writing – review & editing, Resources, Methodology, Data curation, Conceptualization. **Alex Montagne:** Writing – review & editing, Resources, Formal analysis, Data curation. **Corinne Nouveau:** Writing – review & editing, Resources, Project administration, Funding acquisition, Conceptualization. **Faker Bouchoucha:** Writing – review & editing, Supervision, Project administration, Methodology, Conceptualization.

Declaration of competing interest

The authors declare that they have no known competing financial interests or personal relationships that could have appeared to influence the work reported in this paper.

Data availability

Data will be made available on request.

References

[1] A. Kovalev, V. Vakhrushev, B.D. Beake, E.P. Konovalov, D.L. Wainstein, S. A. Dmitrievskii, Damage accumulation phenomena in multilayer (TiAlCrSiY)N/(TiAlCr)N, monolayer (TiAlCrSiY)N coatings and Silicon upon deformation by cyclic nanoindentation, Nanomaterials 12 (2022) 1312, https://doi.org/10.3390/nano12081312.

[2] R. Bauyrzhan, P. Alexander, S. Zhuldyz, B. Dastan, B. Vyacheslav, A. Mukhamedova, Effect of bilayer thickness and bias potential on the structure and properties of (TiZr/Nb)N multilayer coatings as a result of acr-pvd deposition, Materials 15 (2022) 7696, https://doi.org/10.3390/ma15217696, 2022.

[3] Z. Yuan, Y. Han, S. Zang, J. Chen, G. He, Y. Chai, Analysis of the mechanical properties of TiN/Ti multilayer coatings using indentation under a broad load range, Ceram. Int. 47 (2021) 10796–10808, https://doi.org/10.1016/j.ceramint.2020.12.196.

[4] K. Aouadi, C. Nouveau, A. Besnard, M.Chafra B.Tlili, The effect of bilayer periods and their thickness in magnetron sputtering protective multilayer coatig for tribological applications, J. Mater. Eng. Perform. 30 (2021) 2526–2535, https://doi.org/10.1007/s11665-021-05587-6.

[5] A.D. Pogrebnjak, M.A. Lisovenko, A. Turlybekuly, V.V. Buranich, Protective coatings with nanoscale multilayer architecture: current state and main trends, Phys. Usp. 64 (2021) 253, https://doi.org/10.3367/UFNe.2020.08.038823.

[6] J. Tian, Z. Shi, PVD preparation process of (TiN+CrN)/CrAlN superhard nanocomposite multilayer coatings, Adv. Mater. Res. 568 (2012) 368–371, https://doi.org/10.4028/www.scientific.net/AMR.568.368.

[7] B.C. Kang, H.Y. Kim, O.Y. Kwon, S.H. Hong, Bilayer thickness effects on nanoindentation behaviour of Ag/Ni multilayers, Scri. Mater. 57 (2007) 703–706, https://doi.org/10.1016/j.scriptamat.2007.06.038.

[8] S. Kataria, S. Goyal, S. Dash, R. Sandhya, M.D. Mathew, A.K. Tyagi, Evaluation of nano-mechanical properties of hard coatings on a soft substrate, Thin. Solid. Films. 522 (2012) 297–303, https://doi.org/10.1016/j.tsf.2012.09.001.

[9] A. Vereschaka, M. Volosova, A. Chigarev, N. Sitnikov, A. Ashmarin, C. Sotova, J. Bublikov, D. Lytkin, Influence of the thickness of a nanolayer composite coating on values of residual stress and the nature of coating wear, Coatings 10 (2020) 63, https://doi.org/10.3390/coatings10010063.

[10] E. Puchi-Cabrera, M. Staia, A. Iost, Modeling the composite hardness of multilayer coated systems, Thin. Solid. Films. 578 (2015) 53–62, https://doi.org/10.1016/j.tsf.2015.01.070.

[11] K. Rahmoun, A. Iost, V. Keryvin, A multilayer model for describing hardness variations of aged porous silicon low-dielectric-constant, Thin. Solid. Films. 518 (2009) 213–221, https://doi.org/10.1016/j.tsf.2009.07.040.

[12] S.J. Bull, Size effects in the mechanical response of nanoscale multilayer coatings on glass, Thin. Solid. Films. 571 (2014) 290–295, https://doi.org/10.1016/j.tsf.2014.04.014.

[13] H.C. Barshilia, B. Deepthi, N. Selvakumar, A. Jain, K.S. Rajam, Nanolayered multilayer coatings of CrN/CrAlN prepared by reactive DC magnetron sputtering, Appl. Surf. Sci. 253 (2007) 5076–5083, https://doi.org/10.1016/j.apsusc.2006.11.021.

[14] S. Kossman, A. Iost, D. Chicot, D. Mercier, I. Munoz, F. Roudet, P. Dufrenoy, V. Magnier, A. Cristol, Mechanical characterization by multiscale instrumented indentation of highly heterogeneous materials for braking applications, J. Mater. Sci. 54 (2019) 4647–4670, https://doi.org/10.1007/s10853-018-3158-7.

[15] H. Bückle, L'essai de micro dureté et Ses Applications, Publications scientifiques et techniques du ministère de l'air, Paris, 1960. NT90.

[16] B. Jönsson, S. Hogmark, Hardness measurements of thin films, Thin. Solid. Films. 114 (1984) 257–269, https://doi.org/10.1016/0040-6090(84)90123-8.

[17] A. Korsunsky, M. McGurk, S. Bull, T. Page, On the hardness of coated systems, Surf. Coat. Technol. 99 (1998) 171–183, https://doi.org/10.1016/S0257-8972(97)00522-7.

[18] Q. Zhang, X. Li, Q. Yang, Extracting the isotropic uniaxial stress-strain relationship of hyperelastic soft materials based on new nonlinear indentation strain and stress measure, AIP. Adv. 8 (2018) 115013, https://doi.org/10.1063/1.5063384.

[19] M. Dao, N. Chollacoop, K. Van Vliet, T. Venkatesh, S. Suresh, Computational modeling of the forward and reverse problems in instrumented sharp indentation, Acta. Mater. 49 (2001) 3899–3918, https://doi.org/10.1016/S1359-6454(01)00295-6.

[20] X. Xing, Y. Wang, G. Xiao, X. Shu, S. Yu, Y. Wu, Identifying the elastoplastic properties of ductile film on hard substrate, Vacuum. 189 (2021) 110252, https://doi.org/10.1016/j.vacuum.2021.110252.

[21] J.D. Clayton, J.T. Lloyd, D.T. Casem, Simulation and dimensional analysis of instrumented dynamic spherical indentation of ductile metals, Int. J. Mech. Sci. 251 (2023) 108333, https://doi.org/10.1016/j.ijmecsci.2023.108333.

[22] Z. Li, Y. Ye, G. Zhang, F. Guan, J. Luo, P. Wang, J. Zhao, L. Zhao, Research on determining elastic-plastic constitutive parameters of materials from load depth curves based on nanoindentation technology, Micromachines. (Basel) 14 (2023) 1051, https://doi.org/10.3390/mi14051051.

[23] Y.B. Ammar, K. Aouadi, C. Nouveau, A. Besnard, A. Montagne, Identification of the elastic-plastic properties of CrN coating on elastic-plastic substrate by nanoindentation using finite element method-reverse algorithm, Thin. Solid. Films. 756 (2022) 139356, https://doi.org/10.1016/j.tsf.2022.139356.

[24] H. Li, J. Chen, Q. Chen, M. Liu, Determining the constitutive behavior of nonlinear visco-elastic-plastic PMMA thin films using nanoindentation and finite element simulation, Mater. Des. 197 (2021) 109239, https://doi.org/10.1016/j.matdes.2020.109239.

[25] G.Y. He, D.Y. Sun, S.L. Zang, J. Chen, Z.H. Fang, Evaluation of the elastic-plastic properties of TiN coating by nanoindentation technologies using FEM-reverse algorithm, Surf. Coat. Technol. 409 (2021) 126855, https://doi.org/10.1016/j.surfcoat.2021.126855.

[26] M. Karimpour, D.S. Balint, K.A. Rzepiejewska-Malysca, A. Szerling, J. Michler, J. Lin, An inverse method for extracting the mechanical properties of the constituent materials of a multilayer from nanoindentation data, Comput. Mater. Sci. 68 (2013) 384–390, https://doi.org/10.1016/j.commatsci.2012.11.007.

[27] J.J. Kang, A.A. Becker, W. Sun, Determining elastic-plastic properties from indentation data obtained from finite element simulations and experimental results, Int. J. Mech. Sci. 62 (2012) 34–46, https://doi.org/10.1016/j.ijmecsci.2012.05.011.

[28] N. Noii, I. Aghayan, Characterization of elastic-plastic coated material properties by indentation techniques using optimisation algorithms and finite element analysis, Int. J. Mech. Sci. 152 (2019) 465–480, https://doi.org/10.1016/j.ijmecsci.2019.01.010.

[29] K. Bobzin, T. Brgelmann, R.H. Brugnara, M. Arghavani, T.-S. Yang, Y.-Y. Chang, S.-Y. Chang, Investigation on plastic behavior of HPPMS CrN, AlN and CrN/AlN-multilayer coatings using finite element simulation and nanoindentation, Surf. Coat. Technol. 284 (2015) 310–317, https://doi.org/10.1016/j.surfcoat.2015.07.081.

[30] M.Z. Wang, L.B. Gao, K. Cao, J.J. Wu, W.D. Wang, A Bayesian inverse approach to measure the anisotropic plasticity properties of materials using spherical indentation experiment, Measurement 171 (2021) 108812, https://doi.org/10.1016/j.measurement.2020.108812.

[31] T. Csanádi, D. Németh, F. Lofaj, Mechanical properties of Hard W-C Coating on steel substrate deduced from nanoindentation and finite element modeling, Exp. Mech. 57 (2017) 1057–1069, https://doi.org/10.1007/s11340-016-0190-x.

[32] D. Yin, Z. Xu, J. Feng, Y. Qin, Numerical modelling of multilayered coatings-latest developments and applications, Manuf. Rev. 1 (2014) 8, https://doi.org/10.1051/mfreview/2014008.

[33] Y. Gu, W. Chen, C. Zhang, Stress analysis for thin multilayered coating systems using a sinhtransformed boundary element method, Int. J. Solids Struct. 50 (2013) 3460–3471, https://doi.org/10.1016/j.ijsolstr.2013.06.018.

[34] M. Wang, G. Zhang, T. Liu, W. Wang, Determination of elastoplastic properties of 2024 aluminum alloy using deep learning and instrumented nanoindentation experiment, Acta Mech. Solida Sin. 36 (2023) 327–339, https://doi.org/10.1007/s10338-023-00382-3.

[35] X. Long, X. Ding, J. Li, R. Dong, Y. Su, C. Chang, Indentation reverse algorithm of mechanical response for elastoplastic coatings based on LSTM deep learning, Materials 16 (2023) 2617, https://doi.org/10.3390/ma16072617.

[36] X. Long, C. Lu, Z. Shen, Y. Su, Identification of mechanical properties of thin-film elastoplastic materials by machine learning, Acta Mech. Solida Sin. 36 (2022) 13–21, https://doi.org/10.1007/s10338-022-00340-5.

[37] H. Abib, A. Iost, A. Montagne, K. Rahmoun, B. Ayachi, J. Vilcot, Investigations on the mechanical properties of the elementary thin films composing a CuIn1-xGaxSe2 solar cell using the nanoindentation technique, Thin. Solid. Films. 633 (2017) 71–75, https://doi.org/10.1016/j.tsf.2016.11.013.

[38] T. Coleman, M.A. Branch, A. Grace, Optimization Toolbox for Use with MATLAB: User's Guide, Version 2. Math Works, Incorporated, 1999.

[39] G. Papazafeiropoulos, M. Muñiz-Calvente, E. Martínez-Pañeda, Abaqus2Matlab: a suitable tool for finite element post-processing, Adv. Eng. Softw. 105 (2017) 9–16, https://doi.org/10.1016/j.advengsoft.2017.01.006.

[40] M. Lichinchi, C. Lenardi, J. Haupt, R. Vitali, Simulation of Berkovich nanoindentation experiments on thin films using finite element method, Thin Solid Films 312 (1998) 240–248, https://doi.org/10.1016/S0040-6090(97)00739-6.

[41] D. Tabor, The hardness of metals. Oxford classic texts in the physical sciences, Oxford University Press, Oxford, 1951.

[42] Q. Li, L. Yang, Z. Wang, H. Zhang, Z. Liu, Q. Chen, The superior properties of CrN coatingsprepared by high power pulsed reactive magnetron sputtering, AIP. Adv. 10 (2020) 015125, https://doi.org/10.1063/1.5132783.

[43] O. Iracheta, C. Bennett, W. Sun, Characterization of material property variation across an inertia friction welded CrMoV steel component using the inverse analysis of nanoindentation data, Int. J.Mech. Sci. 107 (2016) 253–263, https://doi.org/10.1016/j.ijmecsci.2016.01.023.

[44] R. Snieder, The role of nonlinearity in inverse problems, Inverse Probl. 14 (1998) 387–404, https://doi.org/10.1088/0266-5611/14/3/003.

[45] M. Bazaraa, H. Sherali, C. Shetty, Nonlinear Programming Theory and Algorithms, John Wiley & Sons, Inc. New Jersey, 2006, https://doi.org/10.1002/0471787779.

[46] C. Nouveau, P. Steyer, K. Rao, D. Lagadrillere, Plasma nitriding of 90CrMoV8 tool steel for the enhancement of hardness andcorrosion resistance, Surf. Coat. Technol. 205 (2011) 4514–4520, https://doi.org/10.1016/j.surfcoat.2011.03.087.

[47] A. Munoz, E. Parra, F. Sequeda, CrN coatings deposited by magnetron sputtering: mechanical and tribological properties, DYNA 82 (2015) 147–155, https://doi.org/10.15446/dyna.v82n191.43292.

[48] S. Tien, J. Duh, Effect of heat treatment on mechanical properties and microstructure of CrN/AlN multilayer coatings, Thin. Solid. Films. 494 (2006) 173–178, https://doi.org/10.1016/j.tsf.2005.08.198.

[49] K. Malyska, M. Wojtan, K. Wasmer, K. Hejduk, J. Michler, In-situ SEM indentation studies of the deformation mechanisms in TiN, CrN and TiN/CrN, Micron. 40 (2009) 22–27, https://doi.org/10.1016/j.micron.2008.02.013.

[50] A. Tekaya, H. Ghulman, T. Benameur, S. Labidi, Cyclic nanoindentation and finite element analysis of Ti/TiN and CrNNanocoatings on Zr-based metallic glasses mechanical performance, J. Mater. Eng. Perform. 23 (2014) 4259–4270, https://doi.org/10.1007/s11665-014-1212-4.

[51] E. Cameiro, N. Parreira, T. Vuchkov, A. Cavaleiro, J. Ferreira, M. Andritschky, S. Carvalho, Cr-based sputtered decorative coatings for automotive industry, Materials 14 (2021) 5527, https://doi.org/10.3390/ma14195527.

[52] A. Jallad, A study of the plastic deformation of CrN coatings deposited by RF sputtering, in: M. Chouchane, T. Fakhfak, H. Daly, N. Aifaoui, F. Chaari (Eds.), Design and Modeling of Mechanical Systems - II. Lecture Notes in Mechanical Engineering, Springer, Cham, 2015, pp. 357–364, https://doi.org/10.1007/978-3-319-17527-0_36.

[53] X.Zhang S.Tan, X. Wu, F. Fang, Effect of graded bias on microstructure and hardness of CrN_X films, Adv. Mater. Res. 154-155 (2010) 1476–1480, https://doi.org/10.4028/www.scientific.net/AMR.154-155.1476.

[54] A. Vyas, Z.F. Zhou, Y.G. Shen, Effect of aluminum contents on sputter deposited CrAlN thin films, IOP Conf. Ser.: Mater. Sci. Eng. 307 (2018) 012079, https://doi.org/10.1088/1757-899X/307/1/012079.

[55] Q. Wang, F. Zhou, J. Yan, Evaluating mechanical properties and crack resistance of CrN, CrTiN, CrAlN and CrTiAlN coatings by nanoindentation and scratch tests, Surf. Coat. Technol. 285 (2016) 203–213, https://doi.org/10.1016/j.surfcoat.2015.11.040.

[56] J.C. Lopez, A. Contreras, S. Domingues-Meister, A. Garcia-Luis, M. Brizuela, Tribological behaviour at high temperature of hard CrAlN coatings doped with Y or Zr, Thin. Solid. Films. 55 (2014) 413–420, https://doi.org/10.1016/j.tsf.2013.10.041.

[57] Y. Lv, L. Ji, X. Liu, H. Li, H. Zhou, J. Chen, Influence of substrate bias voltage on structure and properties of the CrAlN films deposited by unbalanced magnetron sputtering, Appl. Surf. Sci. 258 (2012) 3864–3870, https://doi.org/10.1016/j.apsusc.2011.12.048.

[58] K. Bobzin, T. Brogelmann, N.C. Kruppe, M. Arghavani, J. Mayer, T.E. Weirich, On the plastic deformation of chromium-based nitride hard coatings deposited by hybrid dcMS/HPPMS: a fundamental study using nanoscratch test, Surf. Coat. Technol. 308 (2016) 298–306, https://doi.org/10.1016/j.surfcoat.2016.05.093.

[59] M.M. Khakov, L. Xuan, A.V. Tumarkin, A.A. Prosolov, G.A. Kabanov, D.V. Kolodko, B.A. Tarasov, S.M. Irmagambetova, A.V. Kaziev, J. Zhang, Modeling of cracking behavior of CrAlN coatings on silicon during microand nanoindentation, Mater. Chem. Phys. 322 (2024) 129597, https://doi.org/10.1016/j.matchemphys.2024.129597.

[60] K. Bobzin, C. Kalscheuer, M. Carlet, S. Schmauder, V. Guski, W. Verestek, M. Tayyab, 3D deformation modeling of CrAlN coated tool steel compound during nanoindentation, Surf. Coat. Technol. 453 (2023) 129148, https://doi.org/10.1016/j.surfcoat.2022.129148.

[61] K. Bobzin, N. Bagcivan, S. Thieß, J. Perne, Flow curve determination on dc-MS and HPPMS CrAlN coatings, J. Phys. D: Appl. Phys. 46 (2013) 084006, https://doi.org/10.1088/0022-3727/46/8/084006.

[62] T.F. Juliano, M.R. Van Landingham, T. Weerasooriya, P. Moy, Extracting stress-strain and compressive yield stress information from spherical indentation, Army Res. Lab. (2007).

[63] W.C. Oliver, G.M. Pharr, An improved technique for determining hardness and elastic modulus using load and displacement sensing indentation experiments, J. Mater. Res. 7 (6) (1992) 1564–1583, https://doi.org/10.1557/JMR.1992.1564.

[64] A.Y. Adesina, Tribological behavior of TiN/TiAlN, CrN/TiAlN, and CrAlN/TiAlN coatings at elevated temperature, J. Mater. Eng. Perform. 31 (2022) 6404–6419, https://doi.org/10.1007/s11665-022-06722-7.

[65] L.O.C. Lara, J.D.B De Mello, Influence of layer thickness on hardness and scratch resistance of Si-DLC/CrN coatings, Tribol.-Mater., Surf. Interfaces 6 (2012) 168–173, https://doi.org/10.1179/1751584X12Y.0000000019.

[66] A.K. Krella, Cavitation erosion resistance of Ti/TiN multilayer coatings, Surf. Coat. Technol. 228 (2013) 115–123, https://doi.org/10.1016/j.surfcoat.2013.04.016.

[67] M. Falsafein, F. Ashrafizadeh, A. Kheirandish, Influence of thickness on adhesion of nanostructured multilayer CrN/CrAlN coatings to stainless steel substrate, Surf. Interfaces 13 (2018) 178–185, https://doi.org/10.1016/j.surfin.2018.09.009.

[68] X.A. Nie, H.W. Leylan, A.L. Song, Thickness effects on the mechanical properties of micro-arc discharge oxide coatings on aluminium alloys, Surf. Coat. Technol. 116 (1999) 1055–1060, https://doi.org/10.1016/S0257-8972(99)00089-4.

[69] J. Yang, J.J. Roa, M. Odén, M.P. Johansson-Jaesaar, J. Esteve, L. Llanes, Substrate surface finish effects on scratch resistance and failure mechanisms of TiN-coated hardmetals, Surf. Coat.Technol. 265 (2015) 174–184, https://doi.org/10.1016/j.surfcoat.2015.01.038.

[70] G.M. Uddin, A.A. Khan, M. Ghufran, Z.R. Tahir, M. Asim, M. Sagheer, M. Lawad, J. Ahmad, M. Irfan, B. Waseem, Experimental study of tribological and mechanical

properties of TiN coating on AISI 52100 bearing steel, Adv. Mech. Eng. 10 (2018) 1–10, https://doi.org/10.1177/1687814018802.
[71] T. Csanadi, D. Németh, F. Lofaj, Mechanical properties of hard W-C coating on steel substrate deduced from nanoindentation and finite element modeling, Exp. Mech. 57 (2017) 1057–1069, https://doi.org/10.1007/s11340-016-0190-x.
[72] A. Bahri, M. Ellouz, Michaela Klöcker, K. Elleuche, T. Kordisch, Damage evolution of the coating/substrate system TiN/X2CrNi189 under high indentation loads: experimental and numerical study, Int. J. Mech. Mater. Des. 20 (2023) 35–53, https://doi.org/10.1007/s10999-023-09658-5.